Turkish Computational and Theoretical Chemistry

Turkish Comp Theo Chem (TC&TC)

Volume(Issue): 9(1) – Year: 2025 – Pages: 90-114

e-ISSN: 2602-3237

https://doi.org/10.33435/tcandtc.1493008

Received: 01.06.2024 **Accepted:** 05.08.2024 *Research Article*

DFT theoretical calculations on (Z)-2-hydroxy-N'-(4-oxo-1,3-thiazolidin-2-ylidene) benzohydrazide as a methylene tetrahydrofolatereductase inhibitor: An in silico study, molecular docking, and molecular dynamics simulations

Fatima Zohra Boudjenane[a], Rachida Rahmani[a,b], Youcef Megrouss[a,c], Abdelkader Chouaih[a, 1], Nadia Benhalima[a,d,]

[a]Laboratory of Technology and Solid Properties (LTPS), Faculty of Sciences and Technology, AbdelhamidIbnBadis University of Mostaganem, 27000 Mostaganem, Algeria

[b]Department of Process Engineering, Faculty of Sciences and Technology, Ahmed Zabana University of Relizane, 48000 Relizane, Algeria.

[c]Chemistry Department, Faculty of Exact Sciences and Informatics, HassibaBenbouali University, Chlef, 02000, Algeria.

[d]Laboratory of Chemistry: Synthesis, Properties and Applications (LCSPA), Faculty of Sciences, University of Saida - Dr. MoulayTahar, 20000 Saida, Algeria.

Abstract: In this study, (Z)-2-hydroxy-N′-(4-oxo-1,3-thiazolidin-2-ylidene)benzohydrazide (HTBH) was theoretically studied. The B3LYP/6-311G (d, p) level of calculation was performed using the Gaussian 09 program to accomplish the optimal molecular geometry, the global reactivity descriptor parameters, Fukui functions, and molecular electrostatic potential (MEP) parameters. The reduced density gradient (RDG) was calculated with Multiwfn and VMD programs and was used to explore the non-covalent interactions in the molecular system. Furthermore, possible nonlinear optical characteristics were explored. These properties include the electric dipole moment, mean polarizability, and first and second hyperpolarizabilities, indicating the intriguing uses of HTBH in optical systems. The dipole moment of HTBH was calculated to be 6.81 D, while the static second order hyperpolarizability was found to be of 29.86×10^{-36} esu. These parameters have larger values compared to the known nonlinear optical compounds, urea and pNA. In addition, the MEP map provides insight into the electrostatic potential distribution within the molecule, indicating that most nucleophilic and electrophilic regions are around oxygen atoms and the H atom of the hydroxyl group, respectively. The MEP map indicates that the title molecule is capable of undergoing a reaction, particularly through O atoms. Using molecular docking through AutoDockVina software, the inhibitory nature of HTBH against the methylene tetrahydrofolatereductase (MTHFR) protein was analyzed. This enzyme is involved in folate metabolism, and its inhibition can have implications for various biological processes. The docking results indicate that HTBH has a great deal of promise as an inhibitor of MTHFR due to its good binding affinity (-7.2 kcal/mol). Finally, through a detailed molecular dynamics (MD) simulation using the GROMACS 2021 program, we unravel the compound's inhibitory potential and binding characteristics, offering valuable information for developing therapeutic interventions. The binding energies were computed as well by using the MM-PBSA.

Keywords: Benzohydrazides, methylene tetrahydrofolatereductase, docking, hyperpolarizability, molecular dynamics

1. Introduction

Recently, with the development of artificial intelligence, finding novel drugs to treat sickness has been the aim of medicinal chemistry. Developing emerging pharmaceutical compounds is highly complex and requires the knowledge of

[1] Corresponding Authors

e-mail: abdelkader.chouaih@univ-mosta.dz

specialists in many different fields [1]. It has been discovered that heterocyclic organic compounds containing nitrogen atoms in their structure are efficient corrosion inhibitors. Their inhibitory activity has been explained with regard to the quantity of free electron pairs, the π-orbital nature of free electrons, and the density of electrons surrounding the nitrogen atom [2, 3]. Among the heterocyclic aromatic compounds, the thiazolidine derivative has a number of advantages, including a high degree of nonlinear behavior [4]. Additionally, it may yield low aromatics with a higher likelihood of π-electron delocalization between donor-acceptor connections [5]. The push-pull Schiff bases that are generally produced by the condensation of primary amines and active carbonyl groups appear to be specifically created by this heterocycle. Organic material-based nonlinear optical (NLO) systems continue to gain popularity over the years [6]. Conjointly, it is stated that molecules with strong hyperpolarizability can be recognized as NLO materials, which could find applications among semiconductors, data storage, and optical switching [7]. The NLO behavior can be measured by investigating the molecular polarizability and hyperpolarizabilities in static and dynamic modes. Exploring the bioactivity of organic molecules, thiazole derivatives are well-suited molecules to be used as starting materials in the synthesis of essential drugs, such as antibiotics and antiallergic, antiphlogistic, and antitumor substances [8, 9], antimalarials [10], pharmaceuticals [11], biologically interesting antimicrobials [12], protease inhibitors [13], and antischistosomal agents [14]. Hydrazone-based molecular structures with thiazole moiety can have good biological and biochemical activities. Otherwise, the synthetic flexibility of thiazole-hydrazones allows developing a wide variety of biologically relevant derivatives [15, 16]. Furthermore, compounds containing in the same structure phenol, hydrazine, and thiazolidine moieties can also exhibit diverse biological activities based on their specific structures.

The development of novel drugs is being revolutionized by the substantial benefits that drug design and molecular modeling bring to the drug discovery process [17]. In addition, effective methods that improve the efficacy, precision, and success rate of drug discovery are provided by molecular modeling and drug design. On the other hand, they boost up the development process, decrease costs, optimize the properties of new medications, and allow for a rational structure of novel therapeutics [18]. To identify promising drug candidates, molecular modeling can significantly shorten the time required. Before synthesizing and conducting experimental tests, researchers can theoretically evaluate and analyze those using computational models. Furthermore, computational approaches enable the adjustment of pharmacokinetic parameters, such as solubility, stability, and bioavailability, which leads to more successful and secure drugs [19, 20]. Understanding the molecular geometry and electronic properties of molecules is largely dependent on molecular modeling. Essential insights into the structure-function relationships required for rational drug design are provided by this method. In structure-based drug development, molecular docking is a powerful computational approach, which makes it easier to predict the molecular interactions that ligands can have with target proteins [21, 22]. This method not only aids in understanding the binding mechanisms of possible drug candidates but also enables the synthesis of analogs with better pharmacological features [23].

In the present work, we propose a comparative study between experimental results based on X-ray diffraction data of (Z)-2-hydroxy-N′-(4-oxo-1,3-thiazolidin-2-ylidene) benzohydrazide (HTBH) and the corresponding optimized geometry predicted using the Density Functional Theory (DFT) computational method. The investigated compound was previously studied by single-crystal X-ray diffraction technique [24]. DFT is a common approach in theoretical chemistry to study the molecular structure and reactivity of organic molecules. Geometric parameters (bond lengths and bond angles) of the title compound have been evaluated using the DFT method. Additionally, the dipole moment, polarizability, hyperpolarizabilities, and the molecular electrostatic potential (MEP) have also been determined. The Hirshfeld surface (HS) explorations are performed to understand what kind of interatomic contacts give the most significant contributions in crystal structure. The chemical reactivity descriptors, including Fukui functions,

were also calculated to reveal the most molecularly reactive sites. Furthermore, the biological activity and molecular dynamics simulations have also been carried out to screen the inhibitory nature of HTBH against the methylene tetrahydrofolatereductase (MTHFR) protein [PDB ID: 4B4U]. MTHFR is a flavor-protein involved in the metabolism of folate, a B vitamin essential for various cellular processes, including DNA synthesis and methylation. The enzyme helps to convert 5,10-methylenetetrahydrofolate to 5-methyltetrahydrofolate, which is required for the production of methionine and the subsequent generation of S-adenosylmethionine (SAM), a crucial methyl donor [25, 26]. NADPH (nicotinamide adenine dinucleotide phosphate) is a coenzyme involved in numerous metabolic reactions, including the reduction of MTHFR. During the conversion of 5,10-methylenetetrahydrofolate to 5-methyltetrahydrofolate, NADPH transfers electrons to MTHFR. Alternatively, converting homocysteine to methionine is an important step in methionine metabolism, and MTHFR plays a crucial role throughout this process [27]. MTHFR is a transcription factor that promotes the conversion of 5,10-methylenetetrahydrofolate to 5-methyltetrahydrofolate, which is then used as a methyl donor in the remethylation of homocysteine to methionine [28]. MTHFR inhibitors can disrupt the normal functioning of this enzyme. However, it is important to note that NADPH inhibitors directly targeting MTHFR are not widely recognized or commonly used. Several approaches to modulating MTHFR activity or mitigating the effects of MTHFR variants include dietary adjustments, supplementation with specific forms of folate (such as methylfolate), and other strategies to support the methylation cycle. It is advisable to consult with a healthcare professional or a genetic counselor for personalized guidance and recommendations regarding MTHFR-related concerns [29]. The biological activity and MD simulation have been analyzed using the PASSonline (prediction of activity spectra for substances), AutoDockVina, and Gromacs2021.4 programs.

2. Computational Method

2.1. Computational details

The ground-state calculations were carried out using the Gaussian 09 package program [30], and the output files were visualized via Gauss View 5 software [31]. The title molecule's ground state underwent geometry optimization by DFT with B3LYP functional and 6–311 G (d, p) basis set without considering solvation effects. This theoretical model is commonly employed for the prediction of organic compounds' properties, reproducing the experimental geometric parameters [32-36]. The molecular electrostatic surface (MEP) was investigated and visualized. The Multiwfn and VMD programs were used to compute and visualize the reduced density gradient (RDG) and 3D density isosurface [37, 38]. The dipole moment (μ), the mean polarizability (α), the first-order hyperpolarizability (β), and the second-order hyperpolarizability (γ) in the static and dynamic regimes were also computed to evaluate the NLO properties. The NLO parameters are determined using the B3LYP/6-311G(d, p) method, which are reported in atomic units (a.u.) and calculated with the following equations [39]:

$$\mu = (\mu^2_x + \mu^2_y + \mu^2_z)^{1/2}$$

$$\alpha = \frac{1}{3}((\alpha_{xx} + \alpha_{yy} + \alpha_{zz})$$

$$\beta = (\beta 2_x + \beta 2_y + \beta 2_z)^{1/2},$$

where

$\beta_x = (\beta_{xxx} + \beta_{xyy} + \beta_{xzz})$, $\beta_y = (\beta_{yyy} + \beta_{yxx} + \beta_{yzz})$, $\beta_z = (\beta_{zzz} + \beta_{zxx} + \beta_{zyy})$

$$\gamma = \frac{1}{5}(\gamma_{xxxx} + \gamma_{yyyy} + \gamma_{zzzz} + 2\gamma_{xxyy} + 2\gamma_{xxzz} + 2\gamma_{yyzz})$$

The calculated values have been converted into electrostatic units (esu) (for α; 1 au = $0.1482\ 10^{-24}$esu, for β; 1 au = $8.6393\ 10^{-33}$esu).

2.2. PASS analysis

The title compound's biological activity was predicted using the Pass online software. (http://www.way2drug.com/passonline). In this case, the terms "probable activity" (Pa) and "probable inactivity" (Pi) are used to establish the outcomes. When Pa is greater than Pi (Pa > Pi) and Pa is equal to or greater than 0.5 (Pa ≥ 0.5), it suggests that the compound is likely to exhibit the predicted activity.

2.3. Molecular docking

In drug development and pharmaceutical research, molecular docking is a commonly used computational approach. It involves predicting the binding affinity and interaction energy between a receptor and a ligand. Molecular docking provides ligand-protein interaction sites through AutoDockVina **[40]**. AutoDock Tools **[41]** is carried out to prepare the target protein. The docked pose was displayed using Discovery Studio software **[42, 43]**. The MTHFR protein, which is listed in the Protein Data Bank (PDB) under the code 4B4U, is chosen to be inhibited by the title molecule. A grid box in which the ligand can interact with the target protein is formed by the NADPH enzyme active site, which has a grid box size of 40 × 46 × 40 $Å^3$ for x, y, and z, respectively, and a grid center at position -0.3, 10.852, and 31.013 for x, y, and z, respectively. The binding affinity energy is expressed as:

$$E_{Binding} = E_{complex} - (E_{ligand} + E_{protein})$$

where $E_{complex}$ is the total energy of the ligand-protein, and E_{ligand} and $E_{protein}$ are the total energies of the ligand (title molecule) and the receptor (protein), respectively.

2.4. Pharmacokinetic and physicochemical properties

To evaluate the drug-likeness parameters of HTBH, Lipinski's rule of five was applied, which is a widely used method in such studies [44]. The properties of Lipinski's rule of five were obtained using the SwissADME server (http://www.swissadme.ch) [45].

2.5. Molecular dynamics (MD) simulation

To perform the MD simulation, the GROMACS 2021 program was employed [46]. The protein and ligand were docked before the simulation with Auto Dock Vina software to identify the optimal binding conformation as the initial complex structure for MD simulation. The RMSD, Rg, RMSF, SASA, and MM-PBSA parameters were evaluated to obtain the binding energies and consequently the biological activity of the title compound.

3. Results and discussion

3.1. Geometric parameters

Table 1 summarizes the calculated bond lengths and angles compared with experimental data for the molecular structure of HTBH (Figure 1) **[24]**. According to the X-ray data, the C─C average bond length is 1.3836 Å. However, the B3LYP technique calculates a value of 1.39 Å for the benzene cycle with the following bond distances: C1-C2, C2-C3, C3-C4, C4-C5, C5-C6, and C1-C6. Due to the transfer of a lone pair of electrons from the amide nitrogen to the carbon atom, shown in 1.51 and 1.49 Å for the calculated and experimental findings, the bond length of C1-C7 is longer than the other bonds. This single pair may engage with the aromatic ring's pi-system by resonance delocalization. As a result, the carbon atom (C7) undergoes an increase in electron density, increasing the bond between C1 and C7 relative to the other carbon-carbon bonds in benzene. The empirically determined N1–N2 bond distance is 1.38, while the DFT model predicts an analogous bond length of 1.36. This little discrepancy is concentrated in the benzohydrazide fragment. Due to the electron delocalization in the molecule, which gives the C-N bond double bond characteristics, the experimental hydrazide C7-N1 bond length is shorter than the DFT single bond to be 1.33 and 1.37, respectively **[47, 48]**. Based on the literature, a hydrogen bond reduces the C=O bond's double bond nature **[49]**. It improves the C-N bond's double bond character, which accounts for the variations in the lengths of the C7-O2 and C7-N1 bonds discovered at 1.23, 1.21, and 1.33, 1.37 for X-ray and DFT calculations. The values of 121.9, 122.3, 122.8, and 121.2° for O2-C7-N1 and O2-C7-C1 angles suggest that both experimental and theoretical results are in excellent agreement. The experimental values given for the C9-N3-C8 and C8-S1-C10 bond angles of the thiazole ring are 117.45° and 92.28°, respectively, whereas the theoretical values are 119.86° and 91.65°. These results indicate a little disparity between actual and theoretical angles, with the experimental angle being marginally bigger than the theoretical angle **[50]**.

3.2. Frontier molecular orbital analysis

The ionization potential and electron affinities of the molecules, two of the most important quantum chemical features, are related to the HOMO (highest occupied molecular orbital) and the

LUMO (lowest unoccupied molecular orbital). The LUMO, which serves as an electron acceptor, reflects the capacity to receive an electron, while the HOMO represents the capacity to provide one. The molecule's chemical stability is determined by the energy gap between HOMO and LUMO. The HOMO and LUMO schemes for the molecule are shown in Figure 2 as calculated using the B3LYP/6-311G (d, p) level. Additionally, the energy difference between HOMO and LUMO defines their kinetic stability, chemical reactivity, optical polarizability, and chemical hardness **[51]**. The acceptor component is represented by the red phase and the donor area by the green phase. The calculated HOMO and LUMO energies of the title molecule are -6.1579 and 1.4566 eV, respectively, with an energy gap of 4.7013 eV. It is well known that a small energy difference between HOMO and LUMO increases the likelihood of charge transfer inside molecular systems **[52, 53]**. In this work, the charge transfer within the title molecule allows for the precise localization of both donor and acceptor groups. The study of this phenomenon can provide clues for the guided synthesis of more effective inhibitors.

Table 1. Geometrical parameters for HTBH

Bond length (Å)	X-ray	B3LYP	Bond length (Å)	X-ray	B3LYP
C1—C6	1.396	1.401	C7—N1	1.334	1.379
C1—C2	1.400	1.406	C8—N2	1.271	1.267
C1—C7	1.499	1.513	C8—N3	1.383	1.392
C2—O1	1.3630	1.375	C8—S1	1.751	1.799
C2—C3	1.385	1.395	C9—O3	1.219	1.207
C3—C4	1.371	1.389	C9—N3	1.352	1.371
C4—C5	1.380	1.393	C9—C10	1.500	1.529
C5—C6	1.370	1.387	C10—S1	1.806	1.835
C7—O2	1.237	1.214	N1—N2	1.389	1.362
Bond angle (°)	X-ray	B3LYP	Bond angle (°)	X-ray	B3LYP
C6—C1—C2	117.51	117.44	N1—C7—C1	115.70	115.94
C6—C1—C7	116.79	115.04	N2—C8—N3	121.51	120.83
C2—C1—C7	125.68	127.50	N2—C8—S1	127.90	129.30
O1—C2—C3	119.75	119.92	N3—C8—S1	110.58	109.85
O1—C2—C1	119.81	119.38	O3—C9—N3	124.33	125.66
C3—C2—C1	120.45	120.69	O3—C9—C10	123.33	123.97
C4—C3—C2	120.40	120.44	N3—C9—C10	112.33	110.36
C3—C4—C5	120.22	119.85	C9—C10—S1	106.74	108.26
C6—C5—C4	119.64	119.38	C7—N1—N2	121.89	119.48
C5—C6—C1	121.79	122.17	C8—N2—N1	112.77	118.70
O2—C7—N1	121.96	122.84	C9—N3—C8	117.45	119.86
O2—C7—C1	122.33	121.20	C8—S1—C10	92.28	91.65
Torsion angle (°)	X-ray	B3LYP	Torsion angle (°)	X-ray	B3LYP
C6—C1—C2—O1	179.46	179.99	O3—C9—C10—S1	173.59	179.97
C7—C1—C2—O1	−2.4	0.01	N3—C9—C10—S1	−7.08	−0.02
C6—C1—C2—C3	−1.1	0.00	O2—C7—N1—N2	−0.8	−0.01
C7—C1—C2—C3	177.05	179.99	C1—C7—N1—N2	−179.53	179.98
O1—C2—C3—C4	179.98	−179.99	N3—C8—N2—N1	176.65	179.99
C1—C2—C3—C4	0.5	−0.00	S1—C8—N2—N1	−2.5	−0.005
C2—C3—C4—C5	0.4	0.001	C7—N1—N2—C8	174.89	179.95
C3—C4—C5—C6	−0.7	−0.001	O3—C9—N3—C8	−177.67	−179.97
C4—C5—C6—C1	0.1	0.001	C10—C9—N3—C8	3.0	0.027
C2—C1—C6—C5	0.8	0.00	N2—C8—N3—C9	−176.46	179.98
C7—C1—C6—C5	−177.51	−179.99	S1—C8—N3—C9	2.81	−0.02
C6—C1—C7—O2	−6.1	0.01	N2—C8—S1—C10	173.24	179.99
C2—C1—C7—O2	175.83	−179.98	N3—C8—S1—C10	−5.97	−0.001
C6—C1—C7—N1	172.68	−179.98	C9—C10—S1—C8	7.23	0.014
C2—C1—C7—N1	−5.4	0.01			

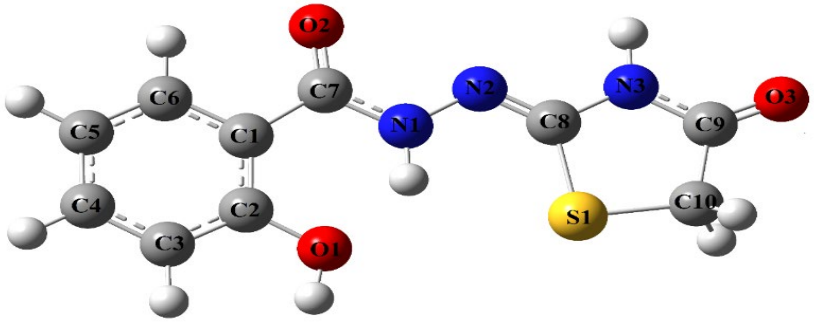

Figure 1. Theoretical structure for HTBH.

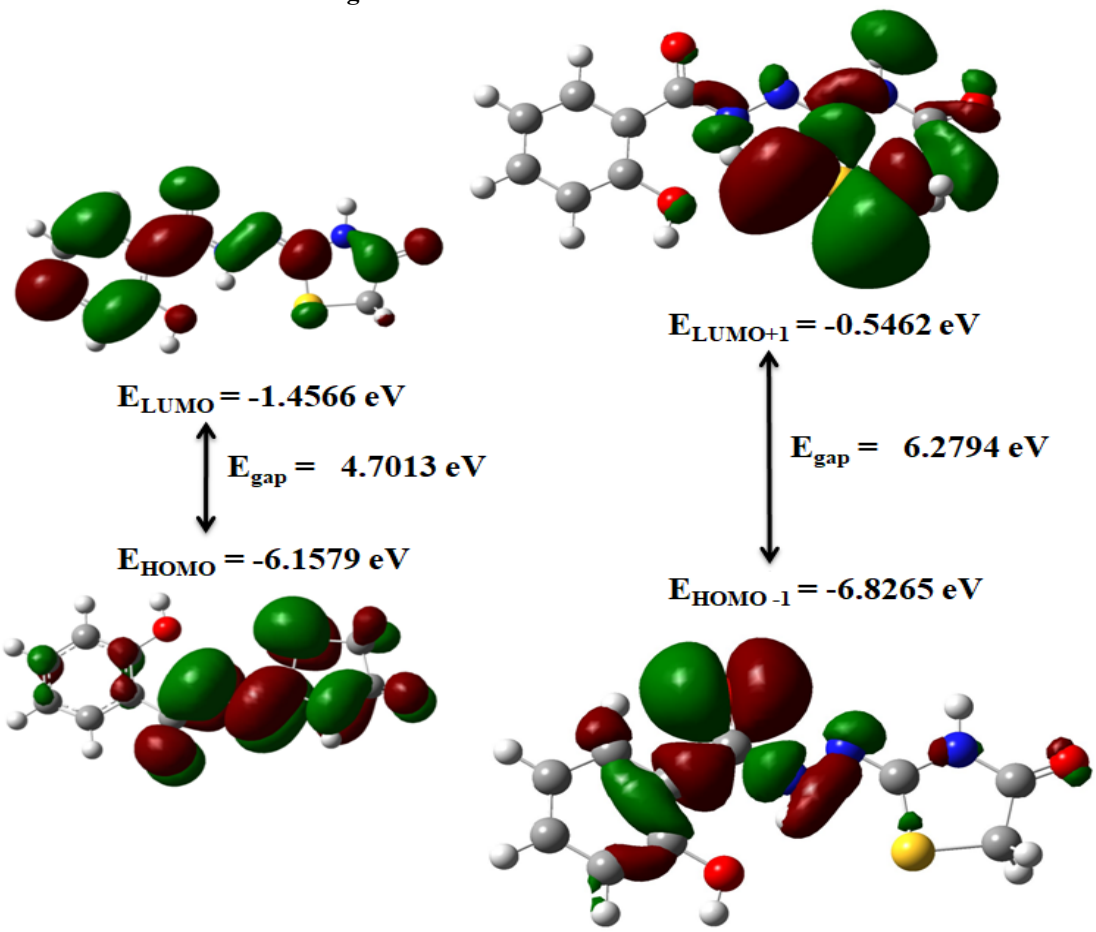

Figure 2. Calculated molecular orbitals for HTBH.

3.3. Global and local chemical reactivity descriptors (GCRDs, LCRDs)

To describe chemical reactivity, the GCRDs and LCRDs parameters were combined with DFT conceptual analysis. The GCRD parameters for the title molecule were computed using the frontier molecular orbital energies [54]. The electronegativity (χ), band gap energy (E), electron affinity (EA), and ionization potential (IP) were calculated using the Koopmann's theorem [55]. Chemical potential (P), global softness (s), index of electrophilicity (ω), and absolute hardness (η) [56] affect a compound's general reactivity and stability are included in Tables 2 and 3. LCRDs have been suggested to define the selectivity or local reactivity of atomic sites in a molecule [57, 58]. The dual descriptor ($\Delta f(r)$), local softness (ΔS), and local electrophilicity indices (ω_k^+ and ω_k^-) were also used in this study. The findings of the FMO study suggest that employing B3LYP/6-311G(d,p) will increase the accuracy of the GCRD parameters. The title compound's ionization potential (IP) and electron affinities (EA) were 1.4566 and 6.1579 eV,

respectively. The molecule tends to draw an electron with a stronger tendency to remove an electron than to lose one. The acquired global softness (S) (1.1753 eV) may be regarded as a low value, whilst the value of the global hardness (η) is the indication of the charge transfer inside the molecule. Thus, the HTBH molecule can be classified as a material with more challenging properties as compared to softer ones. The molecular stability of HTBH could be elucidated by a negative quantity of chemical potential (P) of –3.8073 eV, while the theoretical global electrophilicity index (ω) was 17.0369 eV.

To understand the specific site electrophilic, nucleophilic, or radical character in reactivity of the target molecule and to predict diverse aspects of possible reaction mechanisms or chemical bonding, the local quantities of Fukui functions were studied, which are defined as follows:

$$f_k^+ = q_k(N+1) - q_k(N)$$

For nucleophilic attack on atom

$$f_k^- = q_k(N) - q_k(N-1)$$

For electrophilic attack on atom

$$f_k^0 = \frac{1}{2}[q_k(N+1) - q_k(N-1)]$$

For radical attack on atom k

$$\Delta\omega = \omega(f_k^+ - f_k^-) = \omega\Delta f$$

$$\omega_k^\alpha = \omega f_k^\alpha$$

$$s_k^\alpha = S f_k^\alpha with \alpha = 0; +; -$$

$$\Delta f = f_k^+ - f_k^- = 2q_k(N) - q_k(N+1) - q_k(N-1)$$

$\Delta f > 0$, then, the site is favorable for a nucleophilic attack, whereas if $\Delta f < 0$, then, the site is favorable for an electrophilic attack Based on Table 1. Nucleophilic, electrophilic, and radical reactions are denoted by the signs +, - and 0, respectively. Other uses of the ratio (f_k^+/f_k) and (f_k/f_k^+) as relative nuecleophilicity and relative electrophilicity, respectively were in need to compared to the highest value of (f_k^+/f_k) representing the most probable site of nucleophilic attack.

The thiazole ring's nitrogen atom N1 displays more nucleophilic amounts. However, the S1 atom exhibited the highest electrophilicity among all the multiple charges. To validate these results, the relative nucleo-order electrophilicity was measured. As for the atomic sites' nucleophilic character order: C6 > H4 > C2 > O2 >H9B> C7 > H9A> C12 > C13B >C9 >C13> H13C > H14C. Following is the order of the atomic sites that reveal the electrophilic behaviour: Priority order: H14B > H8 > H5 > H14B > C14 > H2A > H13A > C5 > H4 > H3A N1 > C3 >N2 > O1 H12C > C10 > S1 > C11 > H7 > H12B > H12A. Due to the electronegativity of the carbon, oxygen, and nitrogen atoms, H atoms are electron deficient and vulnerable to nucleophilic attack. It is observed that the electron density surrounding atoms, which are linked to the hydrogen atoms, may contribute to the nucleophilic behavior of the nearby nitrogen atoms. On the other hand, the Fukui functions are computed to show the ability to identify the function or capacity of an electrophile and the electrophilic power of inhibitors.

Table 2. Values of the GCRD parameters for HTBH

Parameters	Energies (eV)
E_H	–6.1579
E_L	–1.4566
Energy gap (ΔE)	4.7013
Ionization potential (IP) $= -E_L$	1.4566
Electron affinity (EA) = $-E_H$	6.1579
Electronegativity (χ) $= \left(\frac{IP+EA}{2}\right)$	3.8073
Chemical potential (P) $= -\left(\frac{IP+EA}{2}\right)$	–3.8073
Chemical hardness (η) $= \frac{1}{2}(E_L - E_H)$	2.3507
Chemical softness (S) $= \frac{1}{2\eta}$	1.1753
Electrophilicity index (ω) $= \frac{\mu^2}{2\eta}$	17.0369

Table 3. Calculated Fukui indices for HTBH.

Atom	f_{0k}	f_{+k}	f_{-k}	Δf	ω_{+k}	ω_{-k}	$\Delta\omega$	S_{+k}	S_{-k}	ΔS
C1	-0.025	-0.0698	0.0197	-0.0895	-1.1883	0.3363	-1.5246	-0.082	0.0232	-0.1052
C2	-0.0264	0.1708	-0.2236	0.3944	2.9101	-3.81	6.72	0.2008	-0.2628	0.4636
C3	-0.0113	-0.1492	0.1265	-0.2757	-2.5412	2.1553	-4.6966	-0.1753	0.1487	-0.324
C4	-0.1108	-0.0987	-0.1229	0.0243	-1.681	-2.0945	0.4135	-0.116	-0.1445	0.0285
C5	0.0083	-0.1207	0.1373	-0.2579	-2.0557	2.3387	-4.3943	-0.1418	0.1613	-0.3031
C6	-0.0698	-0.0804	-0.0591	-0.0213	-1.3699	-1.0069	-0.3631	-0.0945	-0.0695	-0.025
C7	-0.0669	0.3168	-0.4505	0.7673	5.3973	-7.6758	13.0731	0.3723	-0.5295	0.9019
C8	-0.031	0.1757	-0.2377	0.4133	2.9932	-4.0488	7.042	0.2065	-0.2793	0.4858
C9	-0.0312	0.335	-0.3974	0.7324	5.708	-6.7703	12.4783	0.3938	-0.4671	0.8608
C10	0.0018	-0.2816	0.2852	-0.5668	-4.7981	4.8588	-9.6569	-0.331	0.3352	-0.6662
H1	-0.0103	0.2295	-0.2501	0.4796	3.9107	-4.2602	8.1709	0.2698	-0.2939	0.5637
H2	-0.0123	0.09	-0.1146	0.2046	1.5328	-1.9531	3.4859	0.1057	-0.1347	0.2405
H3	-0.01	0.0929	-0.1129	0.2058	1.5834	-1.9233	3.5067	0.1092	-0.1327	0.2419
H4	-0.0133	0.0936	-0.1201	0.2137	1.595	-2.0465	3.6415	0.11	-0.1412	0.2512
H5	-0.006	0.1138	-0.1258	0.2396	1.9388	-2.1429	4.0817	0.1337	-0.1478	0.2816
H6	-0.01	0.1874	-0.2073	0.3946	3.1919	-3.5311	6.7229	0.2202	-0.2436	0.4638
H7	-0.0113	0.1996	-0.2223	0.4219	3.4012	-3.7873	7.1885	0.2346	-0.2613	0.4959
H8	-0.0152	0.1023	-0.1327	0.2349	1.7422	-2.2605	4.0026	0.1202	-0.1559	0.2761
H9	-0.0152	0.1023	-0.1327	0.2349	1.7422	-2.2599	4.0021	0.1202	-0.1559	0.2761
N1	0.0648	-0.1121	0.2418	-0.3539	-1.9098	4.1194	-6.0292	-0.1318	0.2842	-0.4159
N2	0.0342	-0.0746	0.143	-0.2177	-1.2713	2.437	-3.7083	-0.0877	0.1681	-0.2558
N3	0.023	-0.2813	0.3272	-0.6085	-4.7923	5.5743	-10.3666	-0.3306	0.3845	-0.7151
O1	-0.0042	-0.3444	0.3361	-0.6805	-5.8673	5.7254	-11.5928	-0.4048	0.395	-0.7997
O2	-0.0697	-0.3193	0.1799	-0.4993	-5.4406	3.0656	-8.5062	-0.3753	0.2115	-0.5868
O3	-0.0462	-0.323	0.2305	-0.5535	-5.5027	3.9273	-9.4301	-0.3796	0.2709	-0.6505
S1	-0.0362	0.0453	-0.1176	0.1629	0.7714	-2.0037	2.7751	0.0532	-0.1382	0.1914

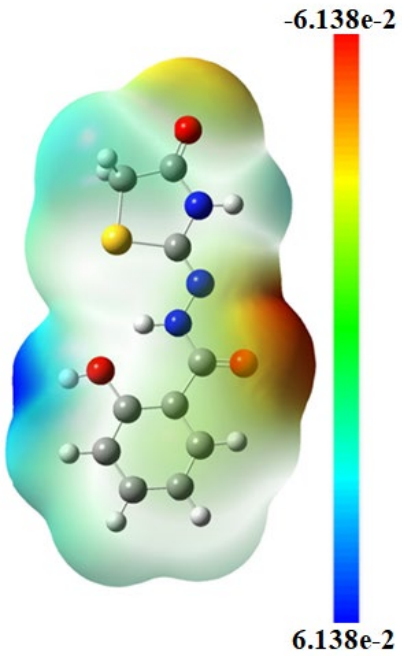

Figure 3. MEP distribution of HTBH.

3.4. MEP description

Reaching the molecular electrostatic potential (MEP), which is correlated with electron density, must be understood to predict how a molecule will interact with another. Accordingly, it is possible to locate probable electrophilic and nucleophilic

regions in the molecule, as well as zones where hydrogen bonds between molecules exist. The electron density can then be used to map the electrostatic potential by representing the potential's value with a color gradation, as it is shown in the following equation [58]:

$$V(r) = \sum \left(\frac{Z_A}{R_A} - r\right) - \int (p(r')/r' - r)\, dr'$$

Z_A is the charge on nucleus A located at R_A, and (R) is the electron density function of the molecule. This equation describes the MEP surfaces that are produced, representing the electrostatic potential V(r) created in the area at each point r around a molecule. Figure 3's color progression from blue to red illustrates the various electrostatic potential values, which rise in the following order: red, yellow, and blue. The blue surfaces indicate the electrophilic site, representing the molecule's most electrostatically positive region. In contrast, the red-colored portion of the mapped surface, known as the nucleophilic site, represents the molecular region with the highest electrostatic potential. The most electronegative regions are located around the oxygen atoms of carbonyl groups, while the most electrophilic regions are situated around the carbonyl groups' oxygen atoms. Otherwise, the most electropositive region is situated especially around the H atom of the hydroxyl group corresponding to the nucleophilic region. It can be concluded based on the MEP map that the title molecule is able to undergo a reaction, especially via O atoms.

3.5. Analysis of non-covalent interactions

The reduced density gradient (RDG) analysis provides valuable information for understanding non-covalent interactions in molecular systems, aiding in designing molecules with desired properties, and is widely used in various fields of chemistry, including organic chemistry, biochemistry, and materials science. The RDG analysis helps study non-covalent interactions in molecular systems, including van der Waals, steric, and hydrogen bonding interactions [59, 60]. The RDG diagrams were generated and plotted as shown in Figure 4. Three colors are observed: green, red, and blue, representing van der Waals, steric (repulsive), and hydrogen bond interactions, respectively. The red region indicates a strong steric effect observed within the atoms of the organic units. This repulsive interaction exhibits a positive sign ($\lambda 2$) ranging from 0.01 to 0.05 a.u. The green and brown bicolored flat regions you mentioned likely indicate regions in the molecular structure with attractive and repulsive interactions. This statement implies that there are regions where atoms or groups interact in a way that promotes closeness (attraction) and regions where they repel each other, potentially due to electronic or steric effects, as seen between hydrazide and thiazolidine fragments. The thiazole and benzene rings' central red spindle forms also show the steric effect caused by the 3D arrangement of atoms or groups in a molecule, which may result in repulsion owing to overlapping electron clouds. Through their effects on bond angles, bond lengths, and molecular conformations, these interactions may affect the whole reactivity. The intramolecular non-covalent interactions are considered weak interactions and are very useful to understand the behavior of molecules towards their activities and especially to investigate the interaction between ligands and the protein receptor.

3.6. Nonlinear optical properties

Focusing on organic molecules' nonlinear optical (NLO) susceptibilities resulting from p electron cloud transfer from donor to acceptor is the goal of this research. Although organic molecules offer these benefits, they also have several NLO drawbacks, such as limited temperature stability and the tendency to relax to random orientation easily [61]. Furthermore, the creation of new fields with altered phase, frequency, amplitude, or other propagation properties from the incident field results from electromagnetic fields interacting in diverse mediums [62].

The total molecular dipole moment, polarizability, and first hyperpolarizability are 6.81 Debye, 2.29×10^{-23} esu and 5.66×10^{-30} esu, respectively, and are depicted in Table 4. The calculated polarizability (α) value is 2.05×10^{-23} esu predicted using B3LYP functional compared to the literature, and considered very acceptable. The polarizability parameters of pNA and urea were reported to be 15.5×10^{-24} and 0.13×10^{-24} esu, respectively [63-65]. The second hyperpolarizability (γ) parameter

of the title molecule is investigated to be 29.86×10^{-36} esu.

The presence of aromatic ring and thiazole moiety in the structure, which serve as donors and acceptors, is confirmed by the significant calculated value of γ. The hydrazide bridge length connecting the molecule's end groups can also be considered a factor in explaining the high value of the first hyperpolarizability. Extending the bridge length between electron donor and acceptor groups can increase a molecule's NLO properties. The site-isolation principle, which states that effective isolation of electron-rich and electron-deficient sites within a molecule can improve NLO effects, was introduced. The improvement of the NLO effects can be ensured by emphasizing the longer bridge which acts as a spacer, prolonging the distance between the accepting and donating groups, limiting electrical interactions, and minimizing NLO effect cancellation [66]. A strong choice for NLO materials, the molecule is suggested by decreasing the HOMO-LUMO energy gap. The dynamic hyperpolarizabilities were also evaluated since observed data are nearly always obtained at incident optical fields. These properties are calculated at ω=911.3 nm to minimize resonance enhancements. The wavelength of 911.3 nm was selected for dynamic NLO calculations based on the previous demonstration indicating that using in-band diode pumping at this wavelength gives rise to a high power continuous-wave (CW) Nd:GdVO4 laser with excellent beam quality [67]. We then presented the quantities β||z (−2ω; ω, ω) for the second-harmonic generation (SHG), β||z (−ω; ω, 0) for electro-optical pockets effect (EOPE), γ (-ω;ω,0,0) for the quadratic electro-optical (dc-Kerr effect), and γ (−2ω;ω,ω,0) for (dc-SHG). As can be seen in Table 4, the dispersion effects of dynamic polarizability α (-ω, ω) are also evaluated to be 2.15×10^{-23} esu. Additionally, the β||z (−ω; ω, 0), β||z (−2ω; ω, ω), γ (-ω;ω,0,0) and γ (−2ω;ω,ω,0) where found to be 6.88×10^{-30}, 1.01×10^{-30}, $37.16\times10^{-36}$and 61.87×10^{-36} esu, respectively.

3.7. Molecular docking and dynamic simulations

3.7.1. PASS and molecular docking analysis

Based on its structural formula, the online PASS program denotes a substance's pharmacological effects, biochemical mechanisms, and specific toxicities. First, the program defines the protein (target) as the receptor for the ligand. Table 5 shows the probable biological activity results for the title molecule, as well as the corresponding probability values. According to the PASS study, the title compound may inhibit the Methylene tetrahydrofolate reductase (MTHFR) protein. NADPH is a key enzyme involved in the synthesis of DNA and RNA, making it essential for cell growth and division [68]. In bacteria, inhibiting NADPH can disrupt their ability to replicate and cause infections, while in cancer cells, targeting NADPH can hinder their uncontrolled growth and proliferation [69]. Therefore, researchers are actively exploring different strategies to design effective inhibitors that selectively target NADPH for both bacterial infections and cancer treatment [70, 71]. The findings have sparked further research into the development of novel thiazole-based compounds with enhanced NADPH inhibitory activity [72, 73]. Moreover, the ability of thiazole-based NADPH inhibitors to target both bacterial and cancer cells makes them promising candidates for dual-purpose therapeutic agents [74]. This information suggests that the protein Methylenetetrahydrofolatereductase (MTHFR), obtained from the Protein Data Bank (PDB) using the code 4B4U, is a potential target for the title compound. The 4B4U code refers to the specific entry in the PDB where the structural information of the protein can be found in literature [75-77]. A high Pa value of 0.731 was chosen for this study. At the same time, the 4B4U protein selection was based on its binding energy value, with negative binding energy indicating good docking ability [78]. Table 6 presents the binding affinities and root-mean-square deviation (RMSD) values for various poses of the ligand within the Methylene tetrahydrofolate reductase (MTHFR) inhibitor protein. The optimal posture for molecular docking is the conformation with the lowest binding energy and an RMSD score of 2.0 [79]. The protein-ligand complex's stability is indicated by its low binding energy, which also verifies the strength of the intermolecular contacts between the ligand and the protein residues. whereas the lowest RMSD (Root Mean Square Deviation) assesses how structurally similar two molecules or complexes are. It describes the binding combinations that are most structurally similar to or well-aligned with the

ligand and target. By considering a 2.0 threshold, binding arrangements where the target and ligand are structurally aligned are examined. In correlation analysis, the coefficients of Pearson and Spearman are employed to assess how well predicted and actual binding affinities within specific structurally related combinations match up. The docking in mode No. 1 resulted in a binding energy (ligand-protein) of −7.2 (kcal/mol), which is consistent with literature results [80]. Table 7 provides an overview of the intermolecular interactions involving the protein residues for the PDB ID: 4B4U and the ligand. The docking results reveal specific intermolecular interactions between the ligand and the protein residue forming. Robust and suitable hydrogen bonds were observed between the O_2 atom of the thiazolidine group in (HTBH) and the SER139, THR141, ALA140, LYS53, GLN97, GLN97, and HIS98 residues. The distances for these hydrogen bonds are 1.959763, 1.73743, 2.663953, 2.174839, 1.928313, 2.491239, and 2.564007 Å, respectively. Additionally, interactions such as electrostatic and hydrophobic were observed between ASP120, TYR49, and N_2 atom, C_6H_4 ring residues, respectively. The 3D intermolecular interactions between the protein and different PDB IDs are highlighted in Fig.5. Based on these docking outcomes, it can be concluded that HTBH has a strong potential as a Methylene tetrahydrofolate reductase (MTHFR) inhibitor.

Table 4. Calculated NLO properties for HTBH.

Dipole moment			
μ_x	0,00		
My	0,00		
Mz	6.81		
μ (Debye)	**6.81**		
Components	Polarizability (0,0)	Polarizability (-w,w) w = 911.3 nm	
α_{xx}	237.62	245.72	
α_{yy}	78.16	79.05	
α_{zz}	148.51	150.92	
‹α› (a.u)	154.76	158.56	
Δα	138.41	144.78	
1 a.u	1.48×10^{-25}	1.48×10^{-25}	
‹α›	2.29×10^{-23}	2.35×10^{-23}	
$\Delta\alpha$(esu)$\times10^{-23}$	**2.05**	**2.15**	
Components	First order hyper-polarizability (0,0,0)	First order hyperpolarizability (-w,w,0) w = 911.3 nm	First order hyperpolarizability (-2w,w,w) w = 911.3 nm
β_{xxx}	549.31	654.15	1039.08
β_{yxx}	92.44	117.76	219.18
β_{zxx}	155.08	27.10	211.93
β_{xyx}	-	173.31	208.30
β_{yyx}	-	34.66	52.44
β_{zyx}	30.12	2.82	42.74
β_{xyy}	20.35	115.71	49.23
β_{yyy}	-6.71	26.47	0.03
β_{zyy}	47.16	-0.67	54.34
β_{xzx}	-	34.20	283.24
β_{yzx}	-	49.52	64.86
β_{zzx}	-	-3.21	-6.69
β_{xzy}	-	187.88	62.0814
β_{yzy}	-	38.69	60.02
β_{zzy}	-	50.67	-6.14
β_{xzz}	6.81303	5.03	3.91
β_{yzz}	-1.95	-2.41	-2.32
β_{zzz}	97.89	91.89	70.52
β_x	576.00	775,00	1092,00
β_y	84.00	142,00	217,00
β_z	300.00	118,00	337,00

‹β› (a.u)	655.31	796.61	1163.37
1 a.u		8.64×10^{-33}	8.64×10^{-33}
‹β›(esu)×10^{-30}	**5.66**	**6.88**	**1.01**
Components	Second order hyper-polarizability (0,0,0,0)	Second order hyperpolarizability (-w,w,0,0);w = 911.3nm	Second order hyperpolarizability (-2w,w,w,0);w 911.3nm
γ_{xxxx}	98.53	123.97	218.57
γ_{xxyy}	7.21	8.97	16.03
γ_{yyyy}	1.12	1.28	1.83
γ_{xxzz}	12.50	15.58	21.27
γ_{yyzz}	1.32	1.59	2.01
γ_{zzzz}	7.55	8.26	10.29
‹γ›(esu) ×10^{-36}	**29.86**	**37.16**	**61.87**

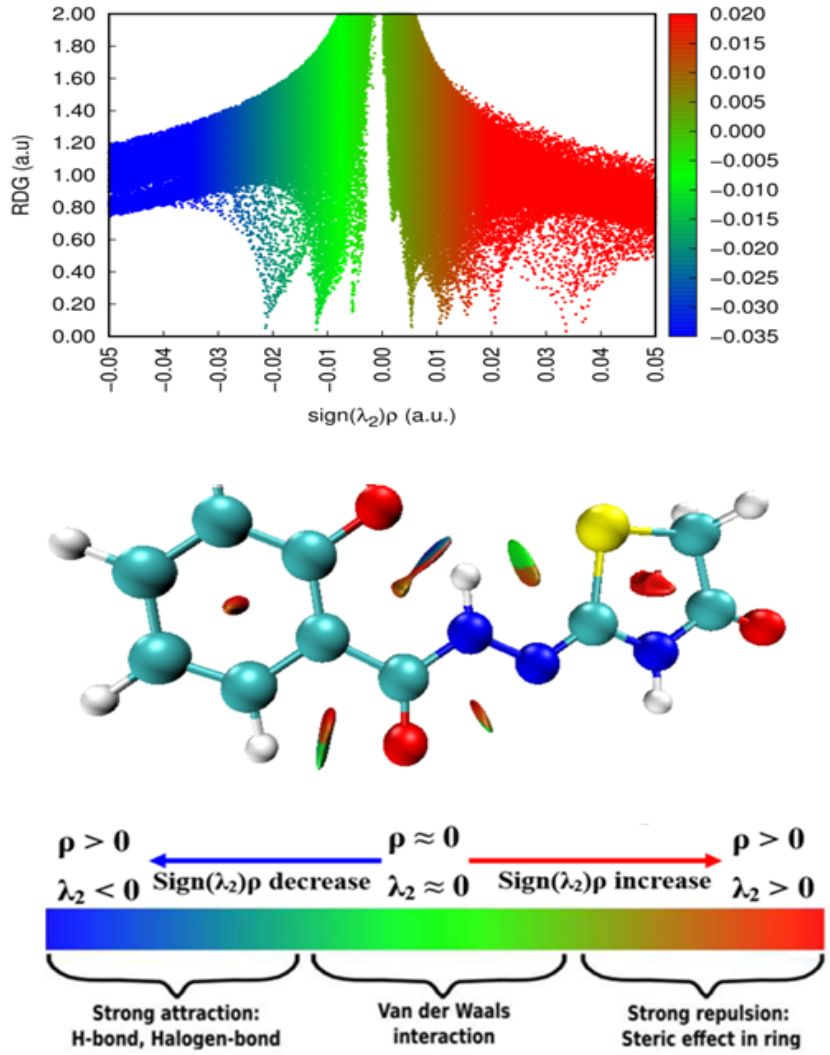

Figure 4. RDG graph of HTBH.

Table 5.PASS results.

Pa	Pi	Activity
0.731	0.027	Methylene tetrahydrofolatereductase (MTHFR) inhibitor
0.7	0.012	Pterindeaminase inhibitor
0.704	0.056	CYP2C12 substrate

0.682	0.061	Testosterone 17beta-dehydrogenase (NADP+) inhibitor
0.603	0.019	Analeptic
0.592	0.014	Mannan endo-1,4-beta-mannosidase inhibitor
0.598	0.026	Phosphatidylserine decarboxylase inhibitor

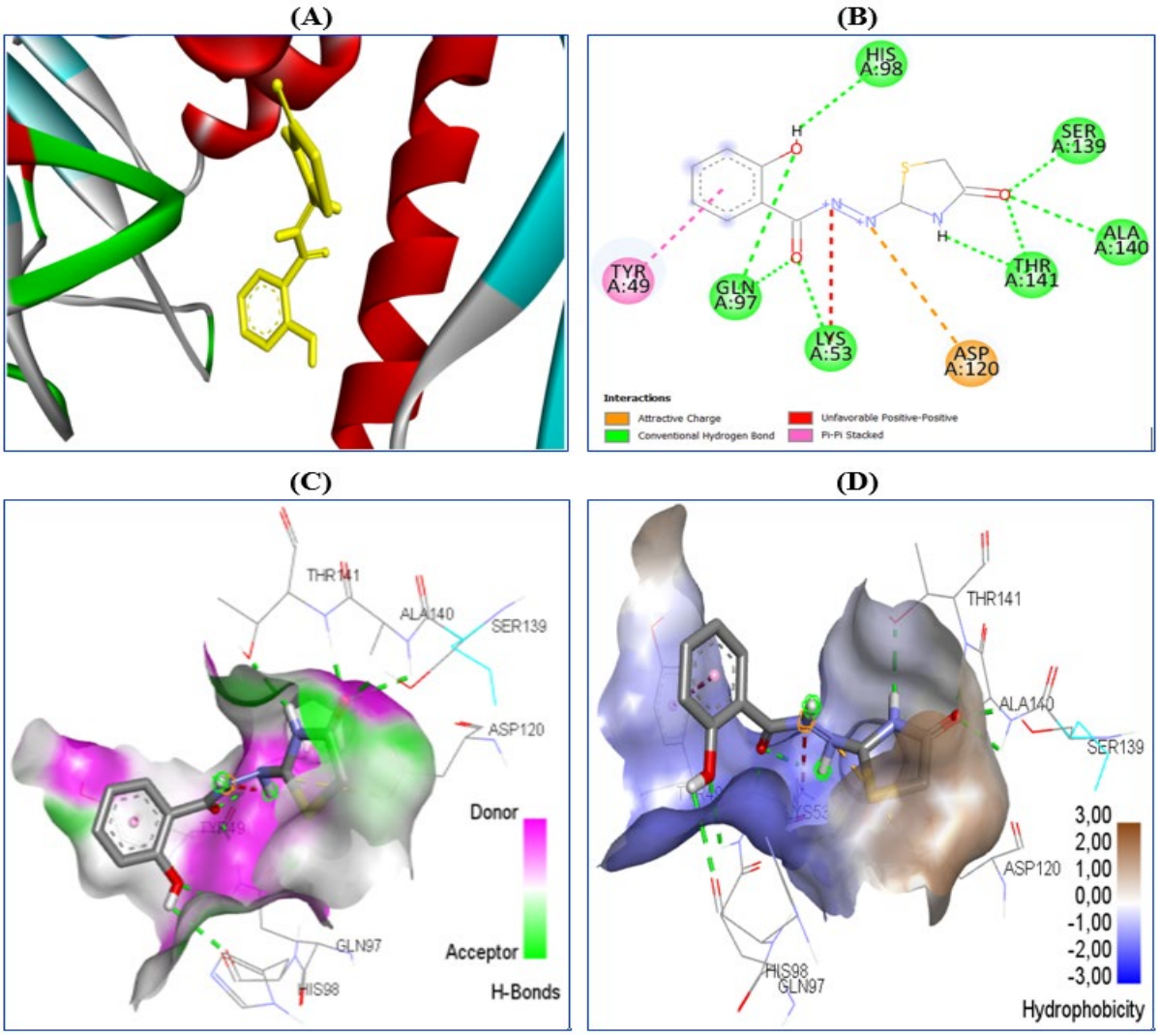

Figure 5. Molecular docking results of HTBH against MTHFR: (A) Docking map, (B)2D interactions, (C) 3D diagram and (D)Hydrophobic activity.

Table 6. Binding affinity and RMSD values of different poses in 4B4U inhibitor of HTBH.

Mode	Affinity (kcal/mol)	Dist from rmsdl.b.	Best mode rmsdu.b.
1	-7.2	0.000	0.000
2	-7.2	6.600	8.317
3	-7.2	6.018	8.327
4	-7.1	1.457	1.972
5	-7.1	2.694	6.277
6	-6.9	2.171	3.086
7	-6.9	2.406	3.396
8	-6.8	3.218	6.280
9	-6.8	3.104	6.495

Table7. Intermolecular interactions involving Methylene tetrahydrofolate reductase (MTHFR) protein residues and HTBH.

Protein	Residue	Compound	Atom/group of compound	Category	Types	Distance (Å)
Methylene tetrahydrofolate reductase (MTHFR) inhibitor(PDB ID : 4B4U)	A:SER139	HTBH	O atom	Hydrogen Bond	conventional hydrogen bond	1.96
	A:THR141		O2 atom	Hydrogen Bond	conventional hydrogen bond	1.74
	A:THR141		C6H4 ring	Hydrogen Bond	conventional hydrogen bond	2.25
	A:ALA140		O2 atom	Hydrogen Bond	conventional hydrogen bond	2.66
	A:LYS53		O2 atom	Hydrogen Bond	conventional hydrogen bond	2.18
	A:GLN97		O2 atom	Hydrogen Bond	conventional hydrogen bond	1.93
	A:GLN97		O2 atom	Hydrogen Bond	conventional hydrogen bond	2.49
	A:HIS98		O atom	Hydrogen Bond	conventional hydrogen bond	2.56
	A:ASP120		N2 atom	Electrostatic	Attractive Charge	4.73
	A:TYR49		C6H4 ring	Hydrophobic	Pi-Pi Stacked	4.26

3.7.2. In silico ADMET investigation

HTBH biological activity was assessed using absorption, distribution, metabolism, excretion, and toxicity (ADMET) analysis. The corresponding pharmacokinetic and physicochemical results are presented in Table 8. The results indicate that HTBH complies with Lipinski's rule of five, suggesting good bioavailability with a score of 0.55 assessing the suitability of a compound as an oral drug. Based on the results, the ligand meets the appropriate requirements for oral drugs.

The bioavailability radar and the BOILED-EGG model of HTBH (Figure 6) depict the red dot's position that indicates unfavorable parameters for blood-brain barrier (BBB) penetration, which can limit its central nervous system effects but is favorable for human intestinal absorption (HIA). In contrast, an unfavorable parameter is observed for the P-gp effect on the molecule, referring to the behavior of the compound, which is a substrate for P-glycoprotein (P-gp), an efflux transporter that can influence drug distribution. The Total Polar Surface Area (TPSA) value of 116.09 Å^2 falls out of the appropriate range, estimating the compound's polar region size that can affect its permeability and transport. A TPSA value less than 90 Å^2 is typically desired for a molecule to penetrate the blood-brain barrier **[81]**. According to the results presented in Table 8, HTBH exhibits a significant skin permeation parameter (Log Kp = -6.62 cm/s), indicating the logarithm of the compound's partition coefficient between octanol and skin. It reflects its potential to penetrate the skin. Furthermore, HTBH has been predicted to have inhibition activity against protease proteins with a probability of 53.3 %, as shown in Figure 7, while the chance of inhibiting lyase is 46.7%. This indicates the potential of HTBH to exhibit inhibitory effects on various biological targets.

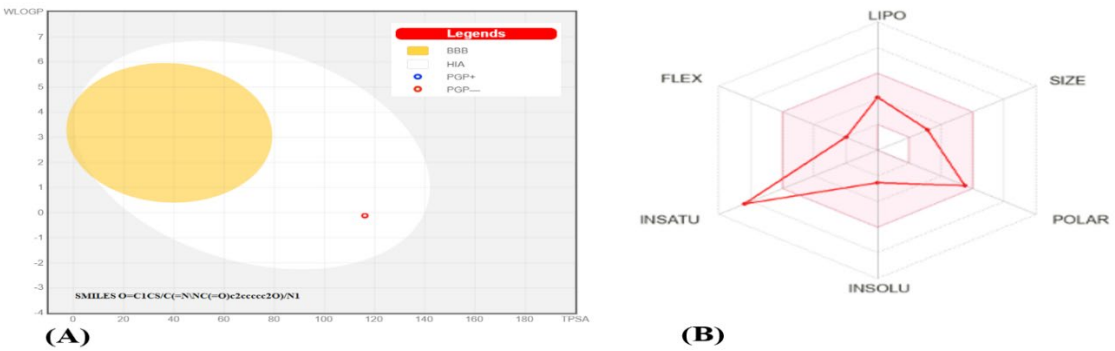

Figure 6. (A) HTBH blood brain barrier (BBB) permeability [BOILED-EGG], and (B) HTBH oral bioavailability radar.

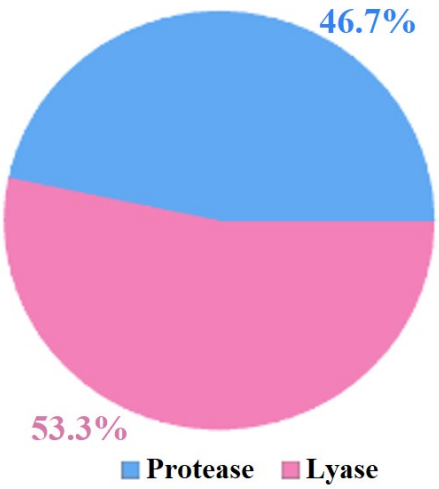

Fig.7. Druggability prediction of HTBH.

Table 8. Physicochemical and pharmacokinetic properties for HTBH.

Physicochemical Properties		***Druglikeness***	
Formula	$C_{10}H_9N_3O_3S$	Lipinski	Yes; 0 violation
Molecular weight	251.26 g/mol	Ghose	Yes
Num. heavy atoms	17	Veber	Yes
Num. arom. heavy atoms	6	Egan	Yes
Fraction Csp3	0.10	Muegge	Yes
Num. rotatable bonds	3	Bioavailability Score	0.55
Num. H-bond acceptors	4	***Lipophilicity***	
Num. H-bond donors	3	Log Po/w (iLOGP)	0.97
Molar Refractivity	67.15	Log Po/w (XLOGP3)	1.71
TPSA	116.09 Å²	Log Po/w (WLOGP)	–0.12
Pharmacokinetics		Log Po/w (MLOGP)	0.51
GI absorption	High	Log Po/w (SILICOS-IT)	0.97
BBB permeant	No	Consensus Log Po/w	0.81
P-gp substrate	No	***Water Solubility***	
CYP1A2 inhibitor	Yes	Log S (ESOL)	–2.54
CYP2C19 inhibitor	No	Solubility	0.727 mg/ml ; 0.0029 mol/l
CYP2C9 inhibitor	No	Class	Soluble
CYP2D6 inhibitor	No	Log S (Ali)	–3.76
CYP3A4 inhibitor	No	Solubility	0.0433 mg/ml ; 0.0002 mol/l
Log Kp (skin permeation)	–6.62 cm/s	Class	Soluble
Medicinal Chemistry		Log S (SILICOS-IT)	–2.74
PAINS	0 alert	Solubility	0.45 mg/ml ; 0.0018 mol/l
Brenk	1 alert: imine-1	Class	Soluble
Leadlikeness	Yes		
Synthetic accessibility	2.77		

3.7.3. Molecular Dynamic (MD) Simulation

In this work, MD simulation is performed to examine the efficiency of ligand binding on protein structure. The MD simulation was performed with the Gromacs 2021 program using the CHARMM36 force field to build the protein topology **[82]**. The CHARMM force field is a powerful tool for simulating protein-ligand interactions by combining force field parameters for proteins and ligands. The ligand and protein are placed together in a simulation box, and force field parameters are applied separately but within the same environment. The non-bonded interactions are calculated using Lenard-Jones and Coulombic potentials, while bonded interactions are considered within the ligand and between the protein and ligand. Simulation protocols like integration algorithms, temperature control, and pressure

control are applied to study the dynamic behavior of the system. The system was solvated using the TIP3P water model and neutralized with Na^+ and Cl^- ions **[83]**. The protein-ligand complex was used as the simulation's starting point, and the HTBH's stability in the protein's binding site was examined. The simulation took place for 100 nanoseconds for temperature (approx. 299 K) and pressure coupling (approx. 1.26 bar), during which the system was designed to utilize as much optimal energy as possible. The steepest descent approach was employed for energy minimization. Position restraint coupled with NVT (100 ps) and NPT (100 ps) ensembles employed the Berendsen thermostat and the Parrinello-Rahman barostat to stabilize the system's both pressure and temperature, respectively **[84, 85]**.

The trajectory of the simulation displayed that the docked ligand remained stable throughout the simulation in the protein's binding site and only exhibited minor conformational changes. The graphical XMGRACE v5.1.19 was used to evaluate the MD simulation data **[86]**. In addition, the built-in capabilities of Gromacs 2021 also served to identify the various vital indicators, such as the root-mean square deviation (RMSD), root mean square fluctuation (RMSF), a radius of gyration (Rg), the H-bonds between protein and the ligand, and interaction energy. These characteristics give crucial insight into the stability and dynamics of the protein-ligand complex and may be utilized to enhance ligand binding in drug development further.

3.7.3.1 The root means square deviation (RMSD)

The root means square deviation (RMSD) is crucial for assessing the variations between confirmations. The greater the RMSD value, the more the deviation **[87-89]**. Figure 8A shows the RMSD of 4B4U (protein) 4B4U - HTBH complex and the ligand HTBH at 100-ns simulation period, respectively. The average RMSDs from 0 to 100 ns for 4B4U (apo form) and 4B4U - HTBH complex are 0.45 nm and 1.52 nm, respectively. During the 100 ns simulation, it is shown that there is an inversing for presenting a discrepancy occur between 601–1752 ps. These RMSD findings demonstrate the relative complex stability throughout the simulation. The RMSD of HTBH (Figure 8A), critical to understanding the ligand's stability in the protein's pocket size, indicated an average of 0.25 nm along 100 ns. These results indicate that both systems reached equilibrium within the simulation time and that the complex was stable throughout the simulation at a simulation time of 11600 ps.

3.7.3.2. The radius of gyration (Rg)

The Rg parameter is a measure of the structural compactness of a protein complex. It provides details on how mass is distributed around the complex's mass center. In MD analysis, Rg is commonly used to evaluate the effectiveness of protein-ligand interaction **[90]**. A stronger value of Rg indicates a less compact and potentially less stable conformation. There was a notable rise in the first 9740 ps followed by stability after this value, the RG values are ranged from 1.92 to 2.02 nm, which is depicted in Figure 8B.

3.7.3.3. The root mean square fluctuation (RMSF)

The RMSF is considered as a measure of the mean deviation of protein residues over a certain period. It provides information about the flexibility or rigidity of different parts of the protein **[91, 92]**. Lower RMSF values denote more rigid or stable zones, while higher values denote substantial variations. Figure 8C shows the protein and ligand RMSF plot. It should be noted that unexpected changes in electron distribution create non-permanent dipoles, primarily used to fit ligands and receptor proteins through steric alignment. Hydrogen bonds form due to van der Waals and electrostatic interactions between hydrogen linked to residues SER139, THR141, THR141, ALA140, LYS53, GLN97, GLN97, HIS98 and an electron-rich atom (oxygen or nitrogen). The energy of these interactions is determined by a Coulomb potential. From the analysis, it is observed that the docked 4B4U significantly presents different minimal fluctuations at various residues level. The binding pocket site of the ligand to 4B4U results in a more stable protein structure with reduced movement and flexibility.

3.7.3.4. The solvent accessible surface area (SASA)

The protein SASA and the complex are illustrated in Figure 8D. The graph shows that the complex exhibits the same deviation and has a lower average value of solvent accessibility throughout the simulation in comparison with the protein form **[93]**. When compared with the isolated protein, the complex has a more folded or compact structure,

with a lower average SASA value suggesting less solvent-accessible surface area. This stability occurs depends on the surface of the complex during simulation, which being less exposed to solvent molecules, ensuring better structural integrity. This indicates that the complex is more stable and maintains a more compact structure during the simulation time.

Table 9. Binding energy and other energy values of complex

Type of energy	Value (kJ/mol)
van der Waals energy	–55.23
Electrostatic energy	–2.85
Polar solvation energy	30.26
Nonpolar solvation energy	–6.35
solvation energy	58.08
Binding energy	–34.2
Temperature	298.15 K

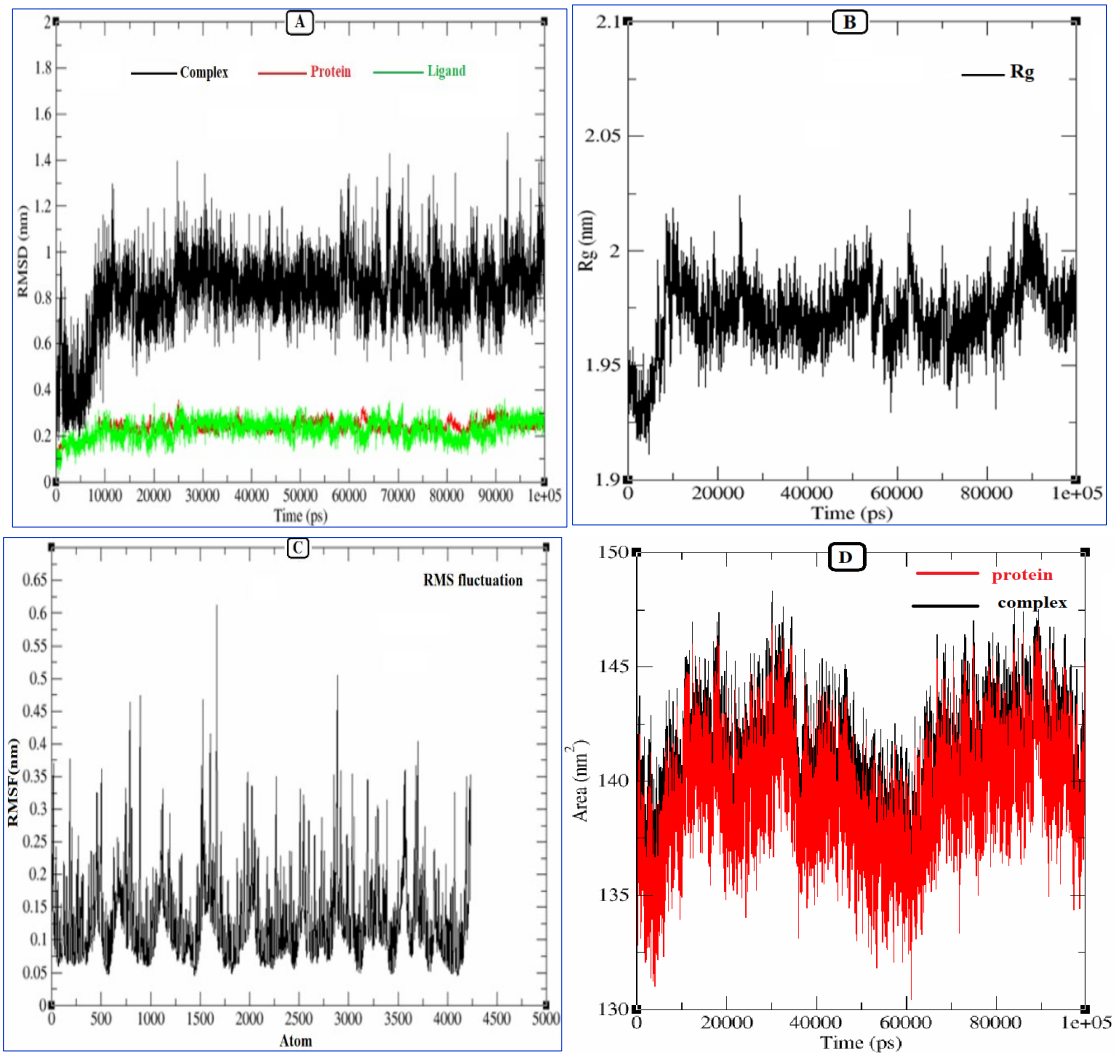

Figure 8. MD simulation trajectories at 100 ns. (A) RMSD, (B) Rg, (C) RMSF, (D) SASA, over the time of simulation. Red: Protein, black: Protein-HTBH complex, green: ligand.

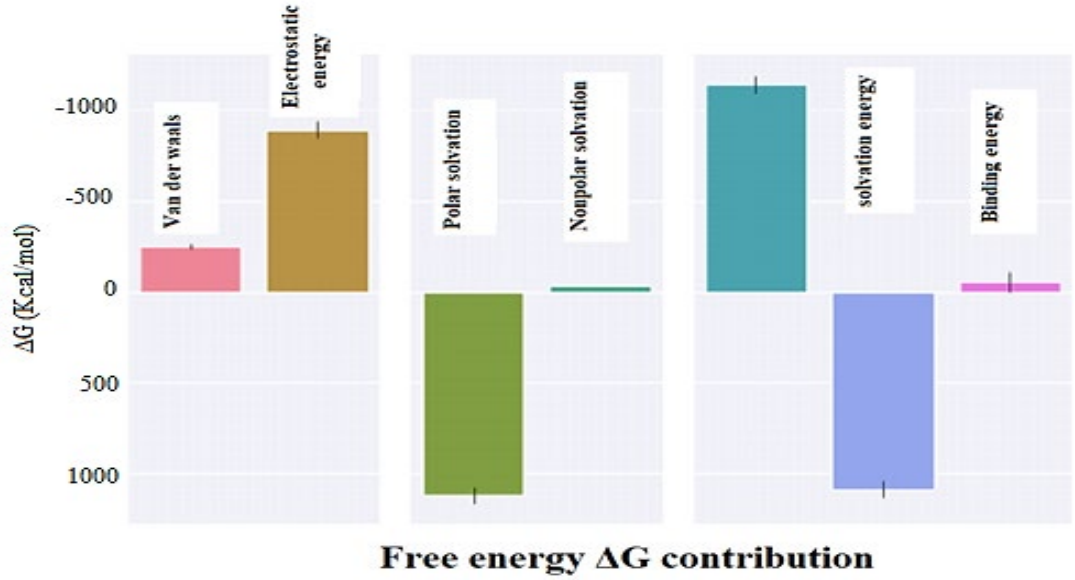

Fig.9. MM-PBSA calculated binding energy for 4B4U-HTBH complex.

3.7.3.5. MM-PBSA

Given the conditions supplied for the complex's environment based on a temporal scaling parameter, the binding energy is computed more precisely using the Poisson-Boltzmann equation and molecular mechanics (MM-PBSA) rather docking. Additionally, the free-energy perturbation (FEP) method [94] was considered in the calculations to avoid net-charge changes and enhance the robustness. Table 9 lists all energy values determined by the MM-PBSA study. For the protein-ligand, 4B4U-HTBH binding energy is –34.2 kJ/mol, while the van der Waals energy is –55.23 kJ/mol, which support the findings of molecular docking. The calculated values are similar to the literature [95]. While the electrostatic interaction is not determined in the outcomes of docking, electrostatic energy was predicted to be –2.85 kJ/mol (Figure 9); this finding demonstrates the MM-PBSA analysis's more accurate prediction of energy levels. The top molecule has energies of 30.26, –6.35, and 58.08 kJ/mol for polar solvation, nonpolar solvation energy, and solvation energies, respectively.

4. Conclusions

In summary, a new heterocyclic compound containing in its structure phenol, hydrazine, and thiazolidine moieties, (Z)-2-hydroxy-N′-(4-oxo-1,3-thiazolidin-2-ylidene)benzohydrazide (HTBH), was extensively studied using the DFT calculation method with B3LYP functional and 6-311G(d,p) basis set. The structure of HTBH was described using geometrical distances and angles. The results of the molecular modeling match well with the previously published experimental X-ray diffraction measurements, confirming the obtained structural model. Theoretical calculations also enabled us to investigate several electronic properties of HTBH. According to the FMO findings, HTBH crystal presents a low gap energy (~ 5 eV) and efficient charge transfer. Furthermore, the GCRD investigation revealed that HTBH has a tougher (2.35 eV) structure, therefore being more reliable. Using dual and multiphilic descriptors, the Fukui functions were employed to highlight the chemically reactive locations, suggesting that hydrogen atoms were susceptible to nucleophilic attack. The regions with the highest electronegative MEP were located around the carbonyl oxygen atoms, and the most electropositive region is situated especially around hydrogen of the hydroxyl group. Strong intermolecular interactions are known to occur in compounds with carbonyl and hydroxyl groups in their structures. Non-covalent interactions were examined using the RDG analysis, revealing that the HTBH structure contains strong and weak interactions, and steric effects. The first and second hyperpolarizabilities, polarizability, and dipole moment of HTBH were

computed to determine its NLO activity. The dipolar moment and polarizability values were 6.81 D and 2.05 × 10^{-23} esu, respectively. In contrast to other well-known NLO compounds such as urea and pNA, HTBH could be suitable for NLO application. The dynamic polarizability at 911.3 nm was also calculated, and the corresponding value was 2.15 × 10^{-23}esu. The static (β(0,0,0)) and dynamic first order hyperpolarizabilities (β(-w,w,0) and β(-2w,w,w)) were calculated to be 5.66, 6.88 and 1.01 × 10^{-30}esu, respectively. Moreover, the static (γ(0,0,0,0)) and dynamic second order hyperpolarizabilities (γ(-w,w,0,0) and γ(-2w,w,w,0)) were calculated to be 29.66, 37.16 and 61.87 × 10^{-36} esu, respectively. According to the above NLO parameters and considering the literature, HTBH has a huge third-order nonlinearity, as indicated by the value of γ. Finally, molecular docking assessments and MD simulation were carried out to establish the binding mode for HTBH around the active area of the receptor. The docking results reveal that HTBH's significant binding affinity of -7.2 kcal/mol enables it to be a potentially attractive MTHFR inhibitor compared to other inhibitors of the same class. The binding energies were also calculated using MM-PBSA, leading to a more accurate prediction of energy levels. HTBH could be a suitable methylene tetrahydrofolate reductase inhibitor.

Acknowledgments

This work was supported by the ministry of higher education and scientific research and the Directorate General for Scientific Research and Technological Development (DG-RSDT).

Disclosure statement

The authors declare that they have no known competing financial interests or personal relationships that could have appeared to influence the work reported in this paper.

References

[1] J. N. Delgado, W. A. Remers, In Textbook of Organic Chemistry Medicinal and Pharmaceutical Chemistry, tenth ed., Wilson and Gisvold, Lippincott Raven, Philadelphia, 1998, 390–348.

[2] M. Alijanianzadeh, A. A. Saboury, M. R. Ganjali, H. Hadi-Alijanvand, A. A. Moosavi-Movahedi, Inhibition of mushroom tyrosinase by a newly synthesized ligand: inhibition kinetics and computational simulations, Journal of Biomolecular Structure and Dynamics 30(4) (2012) 448–459.

[3] M. Kumar Meena, D. Kumar, A. Jayaraj, A. Kumar, K. Kumari, L. M. Katata-Seru, I. Bahadur, V. Kumar, A. Sherawat, P. Singh, Designed thiazolidines: an arsenal for the inhibition of nsP3 of CHIKV using molecular docking and MD simulations, Journal of Biomolecular Structure and Dynamics 40(4) (2022) 1607–1616.

[4] S. Alturk, N. Boukabcha, N. Benhalima, O. Tamer, A. Chouaih, D. Avcı, Y. Atalay, F. Hamzaoui, Conformational, spectroscopic and nonlinear optical investigations on 1-(4-chlorophenyl)-3-(4-chlorophenyl)-2-propen-1-one: a DFT study, Indian J. Phys. 91 (2017) 501–511.

[5] S.H. Masraqui, R.S. Kenny, S.G. Ghadigaonkar, A. Krishnan, M. Bhat-tacharya, Synthesis and nonlinear optical properties of some donor-acceptor oxadiazoles, Das. PK Opt. Mater. 27 (2004) 257–260.

[6] N. Benhalima, N. Boukabcha, O. Tamer, A. Chouaih, D. Avci, Y. Atalay, F. Hamzaoui, Solvent effects on molecular structure, vibrational frequencies; and NLO properties of N-(2,3-Dichlorophenyl)-2-Nitrobenzene Sulfonamide: a density functional theory study, Braz. J. Phys. 46 (2016) 371–383.

[7] O. Kourat, A. Djafri, N. Benhalima, Y. Megrouss, N. E. H. Belkafouf, R. Rahmani, J.-C. Daran, A. Djafri, and A. Chouaih, Synthesis, Crystal Structure, Hirshfeld Surface Analysis, Spectral Characterization, Reduced Density Gradient and Nonlinear Optical Investigation on (E)-N'-(4-Nitrobenzylidene)-2-(Quinolin-8-Yloxy) Acetohydrazide Monohydrate: A Combined Experimental and DFT Approach, J. Mol. Struct. 1222 (2020) 128952.

[8] H. Tanak, M. Yavuz, Molecular structure, spectroscopic (FT-IR and UV-Vis) and DFT quantum-chemical studies on 2-[(2,4-Dimethyl phenyl) iminomethyl] -6-methyl phenol, J. Mol. Struct. 961 (2010) 9–16.

[9] M.M. Ghorab, M.S. Al-Said, Synthesis and antitumor activity of some novel hydrazide,1,2-dihydropyridine, chromene

and benzochromene derivatives, J. Heterocycl. Chem. 49 (2012) 272–280.

[10] B.F. Abdel-Wahab, R.E. Khidre, A.A. Farahat, A.S. El-Ahl, 2-Chloroquinoline-3-aldehyde: synthesis, reactions and applications, Arkivoc 1 (2012) 211–276.

[11] F.M.A. El-Taweel, Novel and Facile Synthesis of Thiophene,2H-Pyran-2-One, Benzimidazo[1,2-A]pyridine and Pyridine Derivatives, Phosphorus, Sulfur and Silicon 179 (2011) 1276–1277.

[12] E. Abd El-Rady, I.H. El-Azab, Reactivity of b-enaminoester of benzo[f] chromene: one pot synthesis of isolated heterocycle-fused derivatives of benzo[f] chromene, Eur. J. Chem. 3 (2012) 81–86.

[13] J. Tois, M. Vahermo, A. Koskinen, Novel and convenient synthesis of 4(1H) quinolones, Tetrahedron Lett. 46 (2005) 735–737.

[14] M.M. Abdelkhalik, A.M. Eltoukhy, S.M. Agamey, M.H. Elnagdi, Enaminones as building blocks in heterocyclic synthesis of nicotinic acid: new synthesis of nicotinic acid and thienopyridine derivatives, J. Heterocycl. Chem. 41 (2004) 431–435.

[15] S. Eswaran, A.V. Adhikari, I.H. Chowdhury, N.K. Pal, K.D. Thomas, New quinoline derivatives: synthesis and investigation of antibacterial and antituberculosis properties, Eur. J. Med. Chem. 45 (2010) 3374–3383.

[16] M.C. Mandewale, B. Thorat, Y. Nivid, R. Jadhav, A. Nagarsekar, R. Yamgar, Synthesis, structural studies and antituberculosis evaluation of new hydrazone derivatives of quinoline and their Zn(II) complexes, J. Saudi Chem. Soc. 22 (2018) 218–228.

[17] A. Ahmed, M. Faisal, In-silico molecular docking, ADME study, and molecular dynamic simulation of new azetidin-2-one derivatives with antiproliferative activity, Turkish Comp Theo Chem (TC&TC) 9(1) (2024) 29–40.

[18] C. Alkaya Yildiz, S. Erkan, Investigation of Anticancer Properties of 2-benzylidene-1-indanone and Its Derivatives by DFT and Molecular Docking, Turkish Comp Theo Chem (TC&TC) 8(2) (2024) 101–109.

[19] J. S. Hannaa, M. M. Jwaidb, K. M. Alawad, In silico screening, molecular dynamic simulation, and pharmacokinetic studies of new Schiff base derivatives from 2-(3-benzoylphenyl) propionic acid as tyrosyl-tRNA synthetase inhibitor, Turkish Comp Theo Chem (TC&TC) 9(1) (2025) 19–28.

[20] Y. Mohammed, A. Al-Hamashi, Identification of Selisistat Derivatives as SIRT1-3 Inhibitors by in Silico Virtual Screening, Turkish Comp Theo Chem (TC&TC) 8(2) (2024) 1–11.

[21] M. Sechi, G. Rizzi, A. Bacchi, M. Carcelli, D. Rogolino, N. Pala, N. Neamati, Design and synthesis of novel dihydroquinoline-3-carboxylic acids as HIV-1 integrase inhibitors, Bioorganic & Medicinal Chemistry 17(7) (2009) 2925-2935.

[22] R. Konakanchi, K. P. Rao, G. N. Reddy, J. Prashanth, Zinc (II) complex: Spectroscopic physicochemical calculations anti-inflammatory and in silico molecular docking studies, J. Mol. Struct. 1263 (2022) 133070.

[23] S. Konduri, V. Pogaku, J. Prashanth, V. Siva Krishna, D. Sriram, S. Basavoju, K. Prabhakara Rao, Sacubitril-Based Urea and Thiourea Derivatives as Novel Inhibitors for Anti-Tubercular against Dormant Tuberculosis, Chemistry Select 6(16) (2021) 3869–3874.

[24] Y. Zhang, P .Li, X .Fan, L .Jin. Crystal structure of (Z)-2-hy-droxy-N'-(4-oxo-1,3-thia-zolidin-2-yl-idene) benzohydrazide, Acta Cryst. E 70 (2014) o1167.

[25] I. Petrone, P.S. Bernardo, Santos, E.C. Dos, E. Abdelhay, MTHFR C677T and A1298C polymorphisms in breast cancer, gliomas and gastric cancer: a review, Genes 12 (2021) 587.

[26] A.R. Velasquez, K.C. Gervacio, D.B. Ramos, E.J. Lugtu, T. Sy-Ortin, P.M. Albano, M.C. Ramos, Methylene tetrahydro folatereductase (MTHFR) 677C>T polymorphisms in breast cancer: A Filipino preliminary case-control study, Gene Reports 29 (2022) 101682.

[27] C. Al Hageh, E. Alefishat, M. Ghassibe-Sabbagh, D.E. Platt, H. Hamdan, R. Tcheroyan, E. Chammas, S. O'Sullivan, A. Abchee, B. Wang, X. Xu, M. Nader, P. Zalloua, Homocysteine levels, H-

Hypertension and the MTHFR C677T genotypes: A complex interaction, Heliyon 9 (2023) e16444.

[28] H.M. Almutairi, N.S. Al-Numair, N.R. Parine, B.O. Almutairi, A.F. Alrefaei, M. Rouabhia, A. Semlali, The protective effects of the methylene tetrahydro folate reductasers 1801131 variant among Saudi smokers, Saudi Journal of Biological Sciences 28(7) (2021) 3972–3980.

[29] J.M. Green, D.P. Ballou, R.G. Matthews, Examination of the role of methylene tetrahydro folate reductase in incorporation of methyltetrahydrofolate into cellular metabolism, The FASEB Journal 2(1) (1988) 42–47.

[30] M.J. Frisch, G.W. Trucks, H.B. Schlegel, G.E. Scuseria, M.A. Robb, J.R. Cheeseman, G. Scalmani, V. Barone, B. Mennucci, G.A. Petersson, Gaussian 09, Revision D.01, Gaussian Inc., Wallingford CT, 2009.

[31] E. Frisch, H.P. Hratchian, R.D. Dennington, T.A. Keith, John Millam, B. Nielsen, A.J. Holder, J. Hiscocks, Gaussian, Syntheses, Structural Elucidation, Thermal Properties, Theoretical Quantum Chemical Studies (DFT) and Biological Studies of BarbituriceHydrazone Complexes Inc. GaussView version 5.0.8, 2009.

[32] S. Bibi, M. Khan, S. ur-Rehman, M. Yaseen, S. Muhammad, R. Nadeem, N. Jahan, S. Noreen, Misbah, Investigation analysis of optoelectronic and structural properties of cis- and trans-structures of azo dyes: density functional theory study, J. Phys. Org. Chem. 34 (2021) e4183.

[33] S. Yahiaoui, A. Moliterni, N. Corriero, C. Cuocci, K. Toubal, A. Chouaih, A. Djafri, F. Hamzaoui, 2-thioxo- 3N-(2-methoxy phenyl) -5 [4'-methyl -3'N -(2'-methoxy phenyl) thiazol-2'(3'H)-ylidene] thiazolidin -4-one: synthesis,characterization, X-ray single crystal structure investigation and quantumchemical calculations, J. Mol. Struct. 1177 (2019) 186–192.

[34] S. Demir, A.O. Sarioğlu, S. Güler, N. Dege, M. Sönmez, Synthesis, crystal structureanalysis, spectral IR, NMR UV-Vis investigations, NBO and NLO of 2-benzoyl-N-(4-chlorophenyl)-3-oxo-3-phenylpropan amide with use of X-ray diffraction studies along with DFT calculations, J. Mol. Struct. 1118 (2016) 316–324.

[35] M. Azayez, S. Chetioui, Y. Megrouss, N. Boukabcha, A. Djedouani, A. R. Guerroudj, N. Meddah Araibi, A. Chouaih, Experimental and theoretical spectroscopic characterization, Hirshfield surface analysis, TD-DFT calculation, and nonlinear optical properties of (E)-1-[(2,4,6tribromophenyl) diazenyl]-naphthalen-2-ol azo dye, J. Mol. Struct. 1261 (2022) 132887.

[36] Ž.B. Milanovic′, Z.S. Markovic′, D.S. Dimic′, O.R. Klisuric′, I.D. Radojevic′, D.S. Šeklic′, M.N. Živanovic′, J.D. Markovic′, M. Radulovic′, E.H. Avdovic′, Synthesis, structural characterization, biological activity and molecular docking study of 4,7-dihydroxycoumarin modified by aminophenol derivatives, Comptes Rendus. Chim. 24 (2021) 215–232.

[37] T. Lu, F. Chen, Multiwfn: a multifunctional wavefunction analyzer, J. Comput. Chem. 33 (2012) 580–592.

[38] W. Humphrey, A. Dalke, K. Schulten, VMD: Visual Molecular Dynamics, Journal of Molecular Graphics 14(1) (1996) 33–8.

[39] R. Rahmani, N. Boukabcha, A. Chouaih, F. Hamzaoui, S. Goumri-Said, On the molecular structure, vibrational spectra, HOMO-LUMO, molecular electrostatic potential, UV–Vis, first order hyperpolarizability, and thermodynamic investigations of 3-(4-chlorophenyl)-1-(1yridine-3-yl) prop-2-en-1-one by quantum chemistry calculation. J. Mol. Struct. 1155 (2018) 484–495.

[40] O. Trott, A.J. Olson, AutoDockVina: improving the speed and accuracy of docking with a new scoring function, efficient optimization, and multithreading, J. Comput. Chem. 31(2) (2009) 455–461.

[41] G.M. Morris, R. Huey, W. Lindstrom, M.F. Sanner, R.K. Belew, D.S. Goodsell, A.J. Olson, AutoDock4 and AutoDockTools4: automated docking with selective receptor flexibility, J. Comput. Chem. 30 (2009) 2785–2791.

[42] Dassault Systèmes BIOVIA, Materials Studio, 7.0, Dassault Systèmes, San Diego, 2017.

[43] W.L. Delano, ThePyMOL molecular graphics development component, Version 1.8, Schrodinger, LLC, New York, 2015.

[44] C.A. Lipinski, Lead- and drug-like compounds: the rule-of-five revolution, Drug Discovery Today: Technologies 1 (2004) 337–341.

[45] A. Daina, O. Michielin, V. Zoete, SwissADME: a free web tool to evaluate pharmacokinetics, drug-likeness and medicinal chemistry friendliness of small molecules, Sci. Rep. 7 (2017) 42717.

[46] H. Bekker, H.J.C. Berendsen, E.J. Dijkstra, S. Achterop, R. van Drunen, D. van der Spoel, A. Sijbers, H. Keegstra, M.K.R. Renardus, Gromacs: A parallel computer for molecular dynamics simulations. In RA. DeGroot, J. Nadrchal (Eds.), World Scientific Publishing, Physics Computing 92 (1993) 252–256.

[47] S.M. Bakalova, A.G. Santos, I. Timcheva, J. Kaneti, I.L. Filipova, G.M. Dobrikov, V.D. Dimitrov, J. Mol. Struct. 710 (2004) 229–234.

[48] H. Marshan Robert, D. Usha, M. Amalanathan, R. Racil Jeya Geetha, M. Sony Michael Mary, Vibrational spectral, density functional theory and molecular docking analysis on 4-nitrobenzohydrazide. J. Mol. Struct. 1223 (2020) 128948.

[49] Q. Gao, G.A. Jeffrey, J.R. Ruble, R.K. McMullan, A single-crystal neutron diffraction refinement of benzamide at 15 and 123 K, Acta Cryst. B47 (1991) 742–745.

[50] F.Z. Boudjenane, F. Triki-Baara, N. Boukabcha, N. E. H. Belkafouf, N. Dege, M. Saidj, N. Khelloul, A. Djafri, A. Chouaih, Synthesis, crystallographic and spectroscopic investigation, chemical reactivity, hyperpolarizabilities and in silico molecular docking study of (Z)-2N-(tertbutylimino)-3N'-(4-methoxyphenyl) thiazolidin-4-one, J. Mol. Struct. 1287 (2023) 135620.

[51] E. Scrocco, J. Tomasi, Electronic molecular structure, reactivity and intermolecular forces: An euristic interpretation by means of electrostatic molecular potentials, Advances in Quantum Chemistry 11 (1979) 115–193.

[52] F.J. Luque, J.M. Lopez, M. Orozco, Perspective on electrostatic interactions of a solute with a continuum. A direct utilization of ab initio molecular potentials for the prevision of solvent effects, Theoretical Chemistry Accounts 103(3–4) (2000) 343–345.

[53] V.A. Adole, B.S. Jagdale, T.B. Pawar, A.B. Sawant, Experimental and theoretical exploration on single crystal, structural, and quantum chemical parameters of (E) -7-(arylidene)-1,2,6, 7-tetrahydro-8 H-indeno[5,4- b] furan-8-one derivatives: A comparative study, Journal of the Chinese Chemical Society 67(10) (2020) 1763–1777.

[54] C.-G. Zhan, J. Nichols, D. Dixon, Ionization potential, electron affinity, electronegativity, hardness, and electron excitation energy: molecular properties from density functional theory orbital energies, The Journal of Physical Chemistry A 107(20) (2003) 4184–4195.

[55] R.G. Parr, R.G. Pearson, Absolute hardness: companion parameter to absolute electronegativity, Journal of the American Chemical Society 105(26) (1983) 7512–7516.

[56] P.K. Chattaraj, S. Giri, S. Duley Update 2 of: Electrophilicity index. Chem. Rev. 111 (2011) PR43–PR75.

[57] R.G. Pearson, Chemical hardness and density functional theory. J. Chem. Sci. 117 (2005) 369–377.

[58] P. Sjoberg, P. Politzer, Use of the Electrostatic Potential at the Molecular Surface to Interpret and Predict Nucleophilic Processes, The Journal of Physical Chemistry 94(10) (1990) 3959–3961.

[59] E.R. Johnson, S. Keinan, P. Mori-Sanchez, J. Contreras-Garcia, A.J. Cohen, W. Yang, Revealing noncovalent interactions, Journal of the American Chemical Society, 132 (2010) 6498–6506.

[60] O. Noureddine, N. Issaoui, M. Medimagh, O. Al-Dossary, H. Marouani, Quantum chemical studies on molecular structure, AIM, ELF, RDG and antiviral activities of hybrid hydroxychloroquine in the treatment of COVID-19: Molecular docking and DFT calculations, Journal of King Saud University – Science 33 (2021) 101334.

[61] R. Rajkumar, A. Kamaraj, S. Bharanidharan, H. Saleem, K. Krishnasamy, Synthesis, spectral characterization, single crystal X-ray diffraction and DFT studies of

4-((2,4,5-triphenyl -1H-imidazole-1- yl) methyl) pyridine derivatives, J. Mol. Struct. 1084 (2015) 74-81.

[62] H. Moghanian, A. Mobinikhaledi, R. Monjezi, Synthesis, spectroscopy (vibrational, NMR and UV-vis) studies, HOMO-LUMO and NBO analysis of 8-formyl-7-hydroxy-4-methylcoumarin by ab initio calculations, J. Mol. Struct. 1052 (2013) 135-145.

[63] C. Adant, M. Dupuis, J. L. Bredas, Ab initio study of the nonlinear optical properties of urea: Electron correlation and dispersion effects. Int. J. Quantum Chem. 56 (1995) 497–507.

[64] L.T. Cheng, W. Tam, S.H. Stevenson, G.R. Meredith, G. Rikken, S.R. Marder, Experimental investigations of organic molecular nonlinear optical polarizabilities.1. Methods and results on benzene and stilbene derivatives, J. Phys. Chem. 95 (1991) 10631-10643.

[65] P. Kaatz, E.A. Donley, D.P. Shelton, A comparison of molecular hyperpolarizabilities from gas and liquid phase measurements, J. Chem. Phys. 108 (1998) 849–856.

[66] Y. Liu, Y. Yuan, X. Tian, J. Yuan, J. Sun. High first-hyperpolarizabilities of thiobarbituric acid derivative-based donor π-acceptor nonlinear optical-phores: Multiple theoretical investigations of substituents and conjugated bridges effect, Int. J. Quantum Chem. 120(10) (2020) e26176.

[67] M. Nadimi, T. Waritanant, A. Major, High power and beam quality continuous-wave Nd:GdVO4 laser in-band diode-pumped at 912 nm, Photonics Res. 5 (2017) 346–349.

[68] G. Gong, X. Gao, J. Wang, D. Zhao, H.S. Freeman, Trisazo Direct Black Dyes Based on Nonmutagenic 3, 3′-Disubstituted Benzidines, Dyes and Pigments 53(2) (2002) 109–117.

[69] Y.I. El-Gazzar, H.H. Georgey, S.M. El-Messery, H.A. Ewida, G.S. Hassan, M.M. Raafat, M.A. Ewida, H.I. El-Subbagh, Synthesis, Biological Evaluation and Molecular Modeling Study of New (1,2,4-Triazole or 1,3,4-Thiadiazole)-Methylthio-Derivatives of Quinazolin-4(3H)-One as DHFR Inhibitors, Bioorganic Chemistry 72 (2017) 282–292.

[70] Y.A. Ammar, S.M.A.A. El-Hafez, S.A. Hessein, A.M. Ali, A.A. Askar, A. Ragab, One-Pot Strategy for Thiazole Tethered 7-Ethoxy Quinoline Hybrids: Synthesis and Potential Antimicrobial Agents as Dihydrofolate Reductase (DHFR) Inhibitors with Molecular Docking Study, J. Mol. Struct. 1242 (2021) 130748.

[71] S.A. Ibrahim, E.A. Fayed, H.F. Rizk, S.E. Desouky, A. Ragab, Hydrazonoyl Bromide Precursors as DHFR Inhibitors for the Synthesis of Bis-Thiazolyl Pyrazole Derivatives; Antimicrobial Activities, Antibiofilm, and Drug Combination Studies against MRSA, Bioorganic Chemistry 116 (2021) 105339.

[72] G.S. Hassan, S.M. El-Messery, F.A.M. Al-Omary, S.T. Al-Rashood, M.I. Shabayek, Y.S. Abulfadl, E.-S.E. Habib, S.M. El-Hallouty, W. Fayad, K.M. Mohamed, Nonclassical antifolates, Part 4. 5-(2-aminothiazol-4-yl)-4-Phenyl-4H-1,2,4-triazole-3-thiols as a new class of DHFR Inhibitors: Synthesis, biological evaluation and molecular modeling study, European Journal of Medicinal Chemistry 66 (2013) 135–145.

[73] P. Gahtori, S.K. Ghosh, P. Parida, A. Prakash, K. Gogoi, H.R. Bhat, U.P. Singh, Antimalarial evaluation and docking studies of hybrid phenylthiazolyl-1,3,5-triazine derivatives: A novel and potential antifolate lead for Pf-DHFR-TS inhibition, Experimental Parasitology 130(3) (2012) 292–299.

[74] H.F. Rizk, M.A. El-Borai, A. Ragab, S.A. Ibrahim, M.E. Sadek, A novel of azo-thiazole moiety alternative for benzidine-based pigments: design, synthesis, characterization, biological evaluation, and molecular docking study, Polycyclic Aromatic Compounds 43(1) (2023) 500–522.

[75] T.C. Eadsforth, F.V. Maluf, W.N. Hunter, *Acinetobacterbaumannii* FolD ligand complexes-potent inhibitors of folate metabolism and a re-evaluation of the structure of LY374571. FEBS J. 279 (2012) 4350–4360.

[76] V.V. Poroikov, D.A. Filimonov, W.-D. Ihlenfeldt, T.A. Gloriozova, A.A. Lagunin,

Y.V. Borodina, M.C. Nicklaus. PASS Biological activity spectrum predictions in the enhanced open NCI database browser. Journal of Chemical Information and Computer Sciences 43(1) (2003) 228–236.

[77] A. Lagunin, A. Stepanchikova, D. Filimonov, V. Poroikov, PASS: prediction of activity spectra for biologically active substances, J. Bioinform. 16 (2000) 747–748.

[78] R.P.D. Bank, RCSB PDB: Homepage. https://www.rcsb.org/.

[79] M. Saidj, A. Djafri, R. Rahmani, N.E.H. Belkafouf, N. Boukabcha, A. Djafri, A. Chouaih, Molecular structure, experimental and theoretical vibrational spectroscopy, (HOMO-LUMO, NBO) investigation, (RDG, AIM) analysis, (MEP, NLO) study and molecular docking of Ethyl-2-{[4-Ethyl-5-(Quinolin-8-yloxyMethyl)-4H-1,2,4-Triazol-3-yl] Sulfanyl} acetate, Polycycl. Aromat. Compd. 43(3) (2023) 2152–2176.

[80] S. Fazil, M. Smitha, Y. Sheena Mary, Y. Shyma Mary, V. Chandramohan, N. Kumar, R. Pavithran, C. Van Alsenoy, Structural (SC-XRD), spectroscopic, DFT, MD investigations and molecular docking studies of a hydrazone derivative, Chemical Data Collections 30 (2020) 100588.

[81] S.A. Hitchcock, L.D. Pennington, Structure-brain exposure relationships, J. Med. Chem. 49(26) (2006) 7559–7583.

[82] T.A. Halgren, Merck molecular force field. III. Molecular geometries and vibrational frequencies for MMFF94, J. Comput. Chem. 17 (1996) 553–586.

[83] W.L. Jorgensen, J. Chandrasekhar, J.D. Madura, Comparison of simple potential functions for simulating liquid water, J. Chem. Phys. 79 (1983) 926–935.

[84] H.J.C. Berendsen, J.P. Postma, W.F.V. Gunsteren, A. DiNola, J.R. Haak. Molecular dynamics with coupling to an external bath, J. Chem. Phys. 81 (1984) 3684–3690.

[85] H.J.C. Berendsen, J.R. Grigera, T.P. Straatsma. The missing term in effective pair potentials, J. Phys. Chem. 91 (1987) 6269–6271.

[86] P. J. Turner. XMGRACE, Version 5.1. 19. Center for Coastal and Land-Margin Research, Oregon Graduate Institute of Science and Technology, Beaverton, OR 2 (2005).

[87] M. Sivaramakrishnan, K. Kandaswamy, S. Natesan, R.D. Devarajan, S.G. Ramakris, Kothandan R .Molecular docking and dynamics studies on plasmepsin V of malarial parasite Plasmodium vivax, Inform Med Unlocked 19 (2020) 100331.

[88] Y.S. Mary, Y.S. Mary, K.S. Resmi, S. Sarala, R. Yadav, I. Celik. Modeling the structural and reactivity properties of hydrazono methyl-4H-chromen-4-one derivatives-wavefunction-dependent properties, molecular docking, and dynamics simulation studies, J. Mol. Model. 27 (2021) 186.

[89] K.S. Jacob, S. Ganguly, P. Kumar, R. Poddar, A. Kumar, Homology model, molecular dynamics simulation and novel pyrazole analogs design of Candida albicans CYP450 lanosterol 14 a-demethylase, a target enzyme for antifungal therapy, J. Biomol. Struct. Dyn. 35 (2017) 1446–1463.

[90] S. Khan, F.I. Khan, T. Mohammad, P. Khan, G.M. Hasan, K.A. Lobb, A. Islam, F. Ahmad, M.I. Hassan, Exploring molecular insights into the interaction mechanism of cholesterol derivatives with the Mce4A: a combined spectroscopic and molecular dynamic simulation studies, Int. J. Biol. Macromol. 111 (2018) 548–560.

[91] L. Martínez, Automatic identification of mobile and rigid substructures in molecular dynamics simulations and fractional structural fluctuation analysis, PloS one 10(3) (2015) e0119264.

[92] B. Pandey, P. Sharma, Structural insights into impact of Y134F mutation and discovery of novel fungicidal compounds against CYP51 in Pucciniatriticina, J. Cell. Biochem. 119 (2010) 2588–2603.

[93] J.S. Al-Otaibi, R.A. Costa, E.V. Costa, V.L. Tananta, Y.S. Mary, Insights into solvation, chemical reactivity, structural, vibrational and anti-hypertensive properties of a thiazolopyrimidine derivative by DFT and MD simulations, Struct Chem. 33 (2022) 1271–1283.

[94] W. Chen, Y. Deng, E. Russell, Y. Wu, R. Abel, L. Wang, Accurate calculation of relative binding free energies between ligands with different net charges, J. Chem. Theory Comput. 14 (2018) 6346–6358.

[95] I. Habib, T. A. Chohan, T.A. Chohan, F. Batool, U. Khurshid, A. Khursheed, A. Raza, M. Ansari, A. Hussain, S. Anwar, N. A. Awadh Ali, H. Saleem, Integrated computational approaches for designing potent pyrimidine-based CDK9 inhibitors: 3D-QSAR, docking, and molecular dynamics simulations,, Computational Biology and Chemistry, 108, (2024) 108003.